

Towed Body Altitude Stabilization and States Estimation in Aerial Recovery of Micro Air Vehicles

Liang Sun * and Randal W. Beard †

In this paper, we present two strategies to stabilize the altitude of the towed body (drogue) in the presence of the steady wind. The flight test results are presented to verify the concept of aerial recovery and the mathematical model of the system. By using the parameter configuration and the data collected in the flight test, a matching work is conducted to testify the fidelity of the mathematical model in the simulation. A series of trade studies are developed in the simulation to analyze the design parameters. In the presence of the steady wind, two proportional-integral controllers are developed to stabilize the altitude of the drogue. The simulation results illustrate the feasibility of the two methods. We also develop an Extended Kalman Filter (EKF) to estimate the drogue states in the case of data delay and the simulation results are presented.

I. Introduction

Micro air vehicles (MAVs) refers to a type of unmanned aerial vehicles (UAVs), with wingspans typically less than 15 inches. With vehicle dimension becoming increasingly small, MAVs have the potential for new applications. Backpackable MAVs can be hand-deployed, but their recovery is problematic in certain scenarios. One potential solution to this problem uses a mothership-cable-drogue system, in which a capture device (drogue) is towed by a larger mothership utilizing a cable, as shown in Figure 1. In this scenario, the mothership enters an orbit designed to cause the towed drogue to execute an orbit of smaller radius and lower speed (less than the nominal speed of the MAV). The MAV then enters the drogue orbit at its nominal airspeed and overtakes the drogue with a relatively slow closing speed. In the terminal stages of rendezvous and capture, a vision-based homing algorithm, such as proportional navigation can be used to close the gap between MAV and drogue.

Based on the dynamic model developed by Sun et al.,¹ a series of trade studies are needed to understand the tradeoffs inherent in the design of the drogue. Different configurations of design parameters, such as drogue aerodynamic drag coefficient, the cable length and the number of links in the cable, will cause different characteristic behaviors of the system. The results of the trade study also guarantee the flight test starts with a feasible setup.

As described by Murray,² in the presence of steady wind, even though the mothership flies in a circular orbit within a horizontal plane, the drogue will enter an inclined elliptical orbit. While the elliptical shape of the orbit can be effectively tracked by the MAV, the altitude variation poses challenges because to rendezvous with the drogue the MAV is required to expend significant energy climbing and descending. To mitigate this problem, we propose two approaches to stabilize the drogue altitude: namely mothership altitude control and cable length regulation.

The drogue in the proposed system has an on-board GPS unit whose signals are sent to the mothership to estimate the drogue orbit parameters. However, the time delay introduced by sending the GPS data to the mothership may be significant enough to adversely affect the guidance strategy of the mothership. We address this problem by using an Extended Kalman Filter (EKF). As presented by Sun et al.,¹ the dynamics of the drogue is derived by Gauss's principle. Although the Gauss's principle regulate the dynamic functions in a relative concise format, the derivation of the EKF for the drogue is nontrivial.

*Ph.D. student, research assistant, Department of Electrical and Computer Engineering, Brigham Young University, Provo, UT 84602, USA. sun.liang@byu.edu

†Professor, Department of Electrical and Computer Engineering, Brigham Young University, Provo, UT 84602, USA. beard@byu.edu .

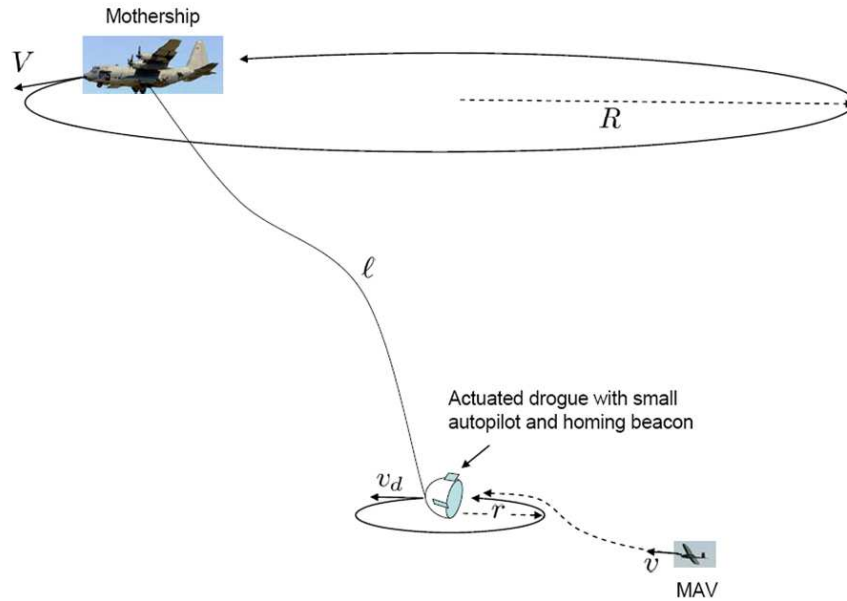


Figure 1: Basic aerial recovery concept. The mothership recovers a MAV by towing a drogue that is actuated and can maneuver and communicate with the MAV to facilitate successful capture.

In Section II, the flight test results are presented to verify the concept of aerial recovery. After that, to testify the fidelity of the mathematical model of the system, the simulation results are applied to match the flight test results. The trade studies are then conducted to analyze the relationship between several key parameters. In Section III, two strategies are proposed to stabilize the drogue altitude and the simulation results are given to show the feasibility of the two methods. In Section IV, an Extended Kalman Filter is developed to estimate the states of the drogue in the case of data delay.

II. Flight test results and trade studies

A. Preliminary Flight Test Results

To validate the mathematical model described by Sun et al.,¹ a series of preliminary flight tests were conducted. In these tests, the mothership (a twin prop, 55 inch wingspan, battery-powered, autonomous aircraft with a Kestrel autopilot) was hand-launched while towing a hemispherical drogue. The mothership and the drogue used for the flight test are shown in Figure 2.

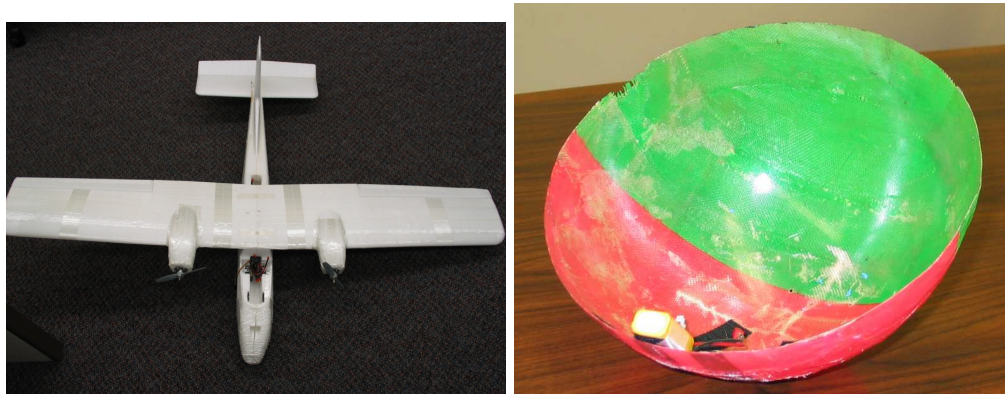


Figure 2: Mothership (left) and hemispherical drogue (right) used in preliminary flight tests

The mothership autonomously maintained a specified circular orbit, and the resulting orbit of the drogue was observed using an on-board GPS data logger. Figure 3 (a) shows the mothership and drogue orbits in the horizontal plane. Figure 3 (b) shows the orbits of the mothership and drogue in the vertical (North-Altitude) plane. Due to the wind, the drogue orbit is tilted out of the horizontal plane, despite the horizontal mothership orbit.

Table 1 gives the system parameters measured by the on-board sensors and GPS. In this case the specified radius of the mothership was approximately 85 m, the mothership airspeed obtained from the on-board autopilot was 14 m/s, and the unstretched cable length was 125 m. The resulting orbit radius and velocity of the drogue were 45 m and 9.9 m/s, respectively. These results illustrate the feasibility of achieving stable drogue orbits at a smaller radius and decreased speed, which is necessary for aerial MAV recovery. It can be seen from the Table 1 that the airspeed and the GPS velocity (ground speed) of the mothership has a difference of about 4.6 m/s with the wind speed magnitude of 0.934 m/s. By using the collected GPS data of mothership or applying the fact that the angular rates of the mothership and the drogue in the steady state are identical, we could calculate the average mothership ground speed which is approximately 18.7 m/s. This difference can result from the error caused by on-board autopilot airspeed port or the error of the wind measurement caused from the constant banking behavior of the mothership. In addition, we used fishing line working as the cable to connect the mothership and the drogue. The distance between the mothership and the drogue during the flight ranges from 130 to 150 meters. Since the cable bent during the flight, it would stretch more than 20 meters.

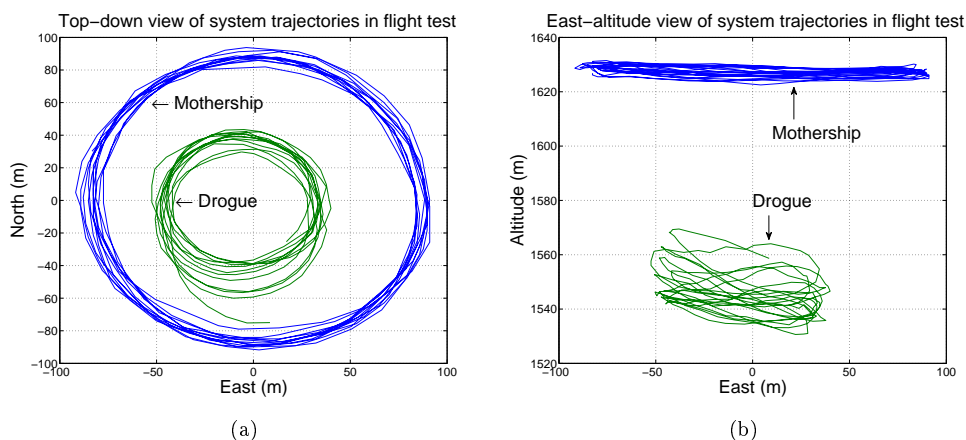


Figure 3: (a) Orbits of mothership and drogue in the horizontal plane in flight test. The mothership (outer) orbit has a radius of 85 m and GPS velocity of 18.7 m/s. The drogue (inner) orbit has a resulting radius of 45 m and a ground speed of 9.9 m/s approximately. (b) Orbits of mothership and drogue in the vertical (East-altitude) plane in the flight test. The mothership (upper) orbit is essentially horizontal, while the drogue (lower) orbit is inclined due to the presence of wind.

B. Matching Simulation Parameters to Flight Test Results

To match our simulator with flight test results we apply the parameters using in the flight test to the simulation. For the airspeed of the mothership, we use 18.7 m/s instead of 13.4 m/s because for a constant wind magnitude of 0.934 m/s applied in the simulation, the airspeed of mothership should approximately equal the averaged ground speed in the flight test. Several parameters such as the drag and lift coefficients of the drogue are tuned to obtain local minima of the errors of both mothership and drogue trajectories. By utilizing the parameters in Table 2, we can obtain Figure 4, which shows the top-down view and side view of the trajectories in the simulation, and Figure 5, which shows the results from simulation overlaid on actual flight test results in north, east and altitude directions respectively. Because of the wind gust and the data measurement error, it is impossible to make simulation and flight test match exactly. However, Figure 4 and Figure 5 show that the simulation model is suitably accurate to conduct trade studies, and for future design work.

Table 1: Flight test parameters

| Mothership | | Drogue | |
|----------------------------------|-----------------|---------------------------|----------------|
| Airspeed (m/s) | | Mass (kg) | 0.159 |
| Measured (Autopilot) | 13.4 | GPS Velocity (m/s) | 9.076 |
| Desired | 14.0 | Center (N, E) (m) | (-2.35, -6.33) |
| GPS Velocity (m/s) | 18.717 | Radius (m) | 42 |
| Center ($North, East$) (m) | (0, 0) | | |
| Radius (m) | 87 | | |
| Wind (averaged) | | Cable | |
| Speed Magnitude (m/s) | 0.934 | Length (m) | 125 |
| Speed in 2D (N, E) (m/s) | (-0.881, 0.109) | Stretched Range (m) | 130 – 150 |

Table 2: Matched simulation parameters

| Mothership | | Drogue | |
|--|----------------------|---------------------------|-----------------|
| Airspeed (m/s) | 18.7 | Velocity (m/s) | 9.2 |
| Radius (m) | 87 | Radius (m) | 44.1 |
| Center (N, E) (m) | (0, 0) | Center (N, E) (m) | (-12.54, -7.43) |
| | | Drag coefficient | 0.24 |
| | | Lift coefficient | 0.28 |
| Wind (constant) | | Cable | |
| Speed Magnitude (m/s) | 0.937 | Length (m) | 130 |
| Speed in 3D ($N, E, Down$) (m/s) | (-0.881, 0.109, 0.3) | | |

C. Preliminary trade studies of the systems

One of the purposes for developing an accurate simulation model is to determine which design parameters are critical for successful aerial recovery. Figures 6, 7 and 8 illustrate some of the trade studies that we conducted. Figure 6 indicates that the (uncontrolled) drogue radius in steady state is strongly dependent on the drag coefficient which ranges from 0.2 to 1.4, but that the drogue orbit altitude is not. This fact informs our design decisions for drogue actuation and control. Figure 7 indicates that radius is also strongly dependent on the mass of the drogue which ranges from 0.159 kg to 2.659 kg , which implies that there will be an abrupt change after the MAV docks with the drogue, and this issue will need to be taken into consideration. Figure 8 indicates that increasing the drag coefficient with a fixed mass results in a lower drogue orbit altitude and radius, and increasing the mass, which ranges from 0.159 kg to 2.659 kg with a fixed drag coefficient results in larger drogue orbit altitude and radius.

III. Drogue altitude stable control

In Reference 1, we should see that the drogue maintains a horizontal circular orbit in the absence of wind. However, in the presence of a constant wind, the orbit of the drogue will be an inclined elliptical orbit, major axis aligned with the (constant) wind vector as shown in Figure 3. Figure 9 shows the altitude of the drogue in simulation where it can be seen that the altitude oscillates approximately 6 m when the constant wind has a magnitude of 1.12 m/s . In this section, we will develop two strategies to stabilize the drogue altitude.

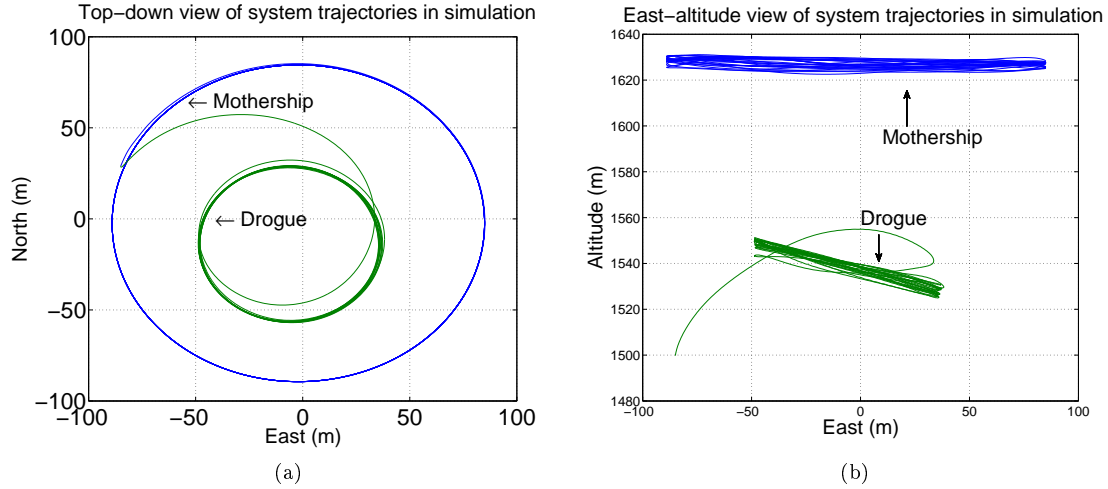


Figure 4: (a) Orbits of mothership and drogue in the horizontal plane in the simulation; (b) Orbits of mothership and drogue in the vertical (East-altitude) plane in the simulation.

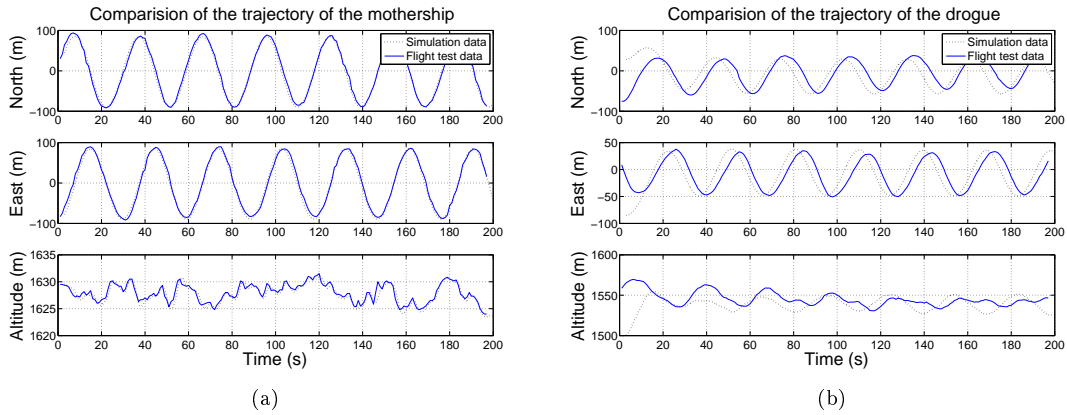


Figure 5: (a) Comparison of mothership data in the simulation and in the flight test; (b) Comparison of drogue data in the simulation and in the flight test

A. Drogue altitude stabilization using mothership altitude control

The first method that we will explore for stabilizing the drogue altitude, is to vary the mothership altitude based on a feedback signal from the drogue. Accordingly, we use the PI controller

$$\ddot{h}_d^m = \left(K_P^h + \frac{K_I^h}{s} \right) (h_c^{dr} - h_d^{dr}), \quad (1)$$

where \ddot{h}_d^m is the desired acceleration of the mothership in the altitude, h_c^{dr} and h_d^{dr} are the current and desired altitudes of the drogue respectively, and K_P^h and K_I^h are positive control gains.

Figure 10 shows the resulting drogue altitude where the mothership altitude is controlled using (1) which is switched on at $t = 65$ s. The oscillation of the drogue altitude reduces to approximately 1.2 m. Figure 11 depicts the corresponding mothership altitude which oscillates within approximately 8 m. Since mothership-cable-drogue system is not a rigid body, the drogue response is delayed. Thus, this approach can only mitigate the drogue altitude oscillation to some extent, but cannot totally eliminate it.

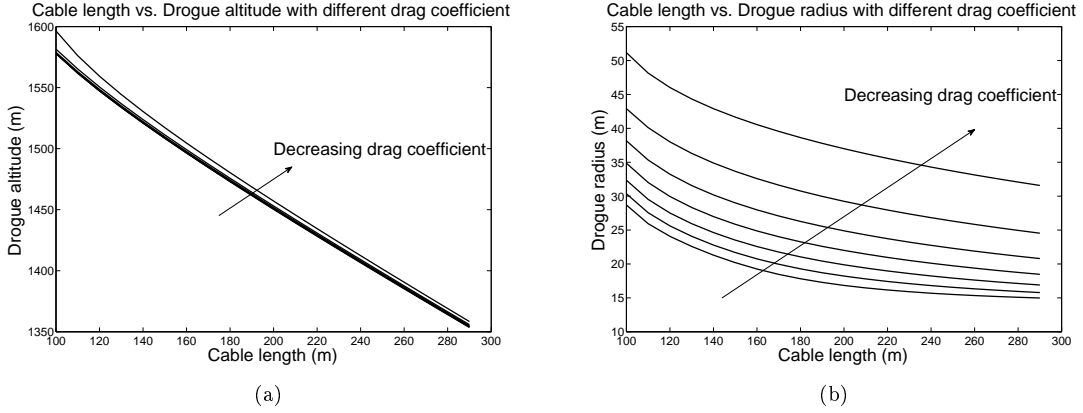


Figure 6: Cable length vs. Drogue altitude and radius with different drag coefficient.

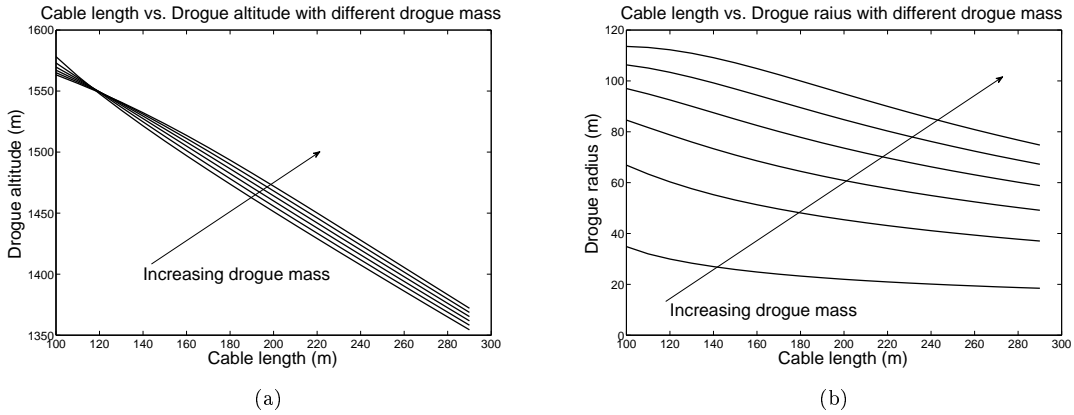


Figure 7: Cable length vs. Drogue altitude and radius with different drogue mass.

B. Drogue altitude stabilization using cable length regulation

The second method that we will explore for drogue altitude regulation is motivated by Figure 6 (a), which show that the altitude of the drogue is highly sensitive to the length of the cable. Therefore, adding a winch to the drogue that can regulate the length of the cable will likely be an effective method to regulate drogue altitude. We propose using the PI controller

$$\dot{\ell}^d = \left(K_P^\ell + \frac{K_I^\ell}{s} \right) (h_c^{dr} - h_d^{dr}), \quad (2)$$

where $\dot{\ell}^d$ is the cable length rate (winch speed), h_c^{dr} and h_d^{dr} are the current and desired altitudes of the drogue respectively, and K_P^ℓ and K_I^ℓ are the positive control gains.

The winch will likely have relatively slow dynamics, which will be effective for removing the incline in the orbit, but will not be effective for suppressing high frequency variations in the altitude. These will be actuated using a mechanism at the cable attachment point to maintain constant roll angle of the drogue and handle high bandwidth regulation of altitude.

Figure 12 shows the drogue altitude using (2) which is switched on at $t = 65$ s. The oscillation of the drogue altitude reduces to about 0.3 m. To achieve this result, the winch speed lower limit is 0.5 m/s. The cable length regulation range is approximately 16 m, which may not be realizable.

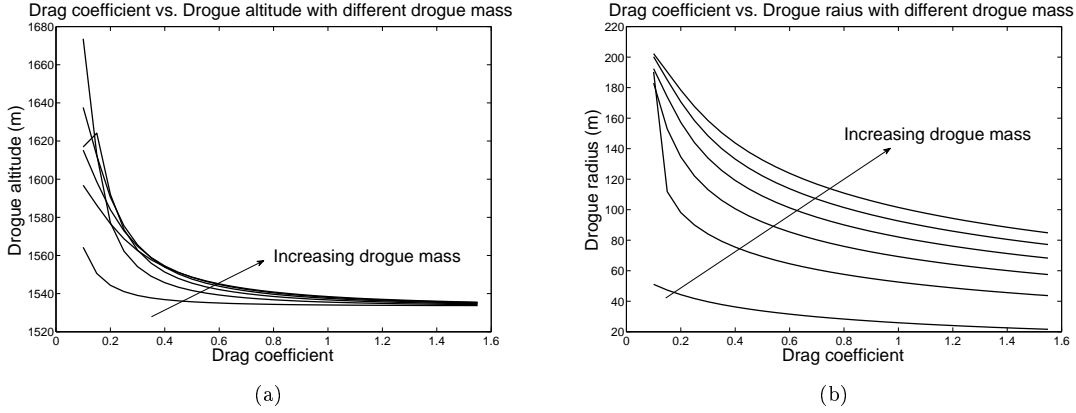


Figure 8: Drogue drag coefficient vs. Drogue altitude and radius with different drogue mass.

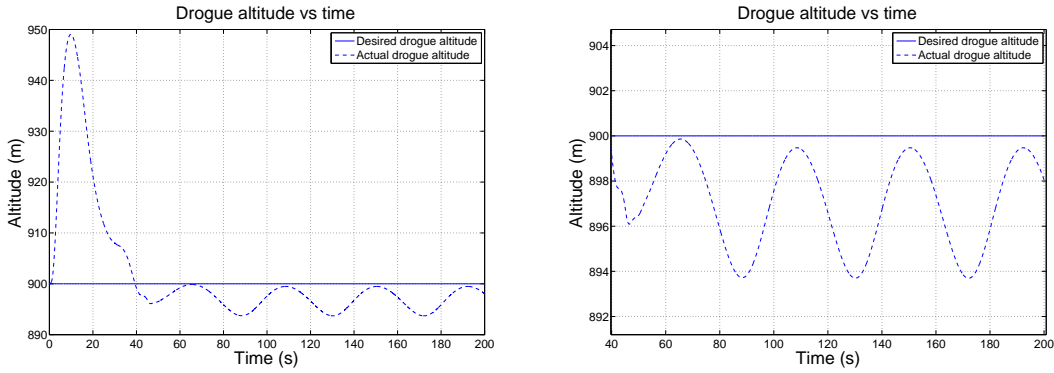


Figure 9: Drogue altitude vs. time in the presence of wind under no stable control (left). From the zoomed-in view (right), it can be seen that in the steady state, the drogue altitude oscillates over the range of approximately 6 m.

C. Drogue altitude stabilization using both mothership altitude control and cable length regulation

Figures 14, 15 and 16 depict the drogue altitude, mothership altitude and cable length in the presence of wind under altitude stabilization using both mothership altitude control and cable length regulation. The oscillation of the drogue altitude reduces to 0.02 m . The mothership altitude oscillation decreases to about 7 m and the cable length regulation reduces to about 1 m .

IV. Drogue states estimation using Extended Kalman Filter

To stabilize the drogue altitude, the drogue position data is essential. Receiving the data from a GPS logger results in data delay since the sample time is about 1 second and sometimes the connection is lost. We will develop a method to estimate the drogue states using Extended Kalman Filter (EKF).

A. Drogue states estimation using EKF

To simplify the problem, we employ the single-link cable model, and the dynamics for the drogue are derived by applying the Gauss's Principle.¹ If the N -link ($N > 1$) cable model is used, we can replace the mothership states with the states of the $(N - 1)^{th}$ joint, and similar results will be obtained.

Let \mathbf{x}_m and \mathbf{x}_d be the positions of the mothership and drogue in the inertial frame respectively. The

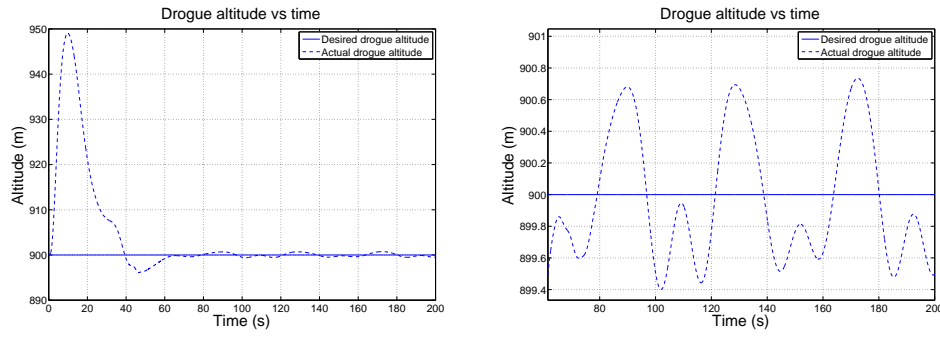


Figure 10: Drogue altitude vs. time in the presence of wind under stable control strategy using mothership altitude control (left). From the zoomed-in view (right), it can be seen that in the steady state, the drogue altitude oscillates over the range of approximately 1.2 *m*.

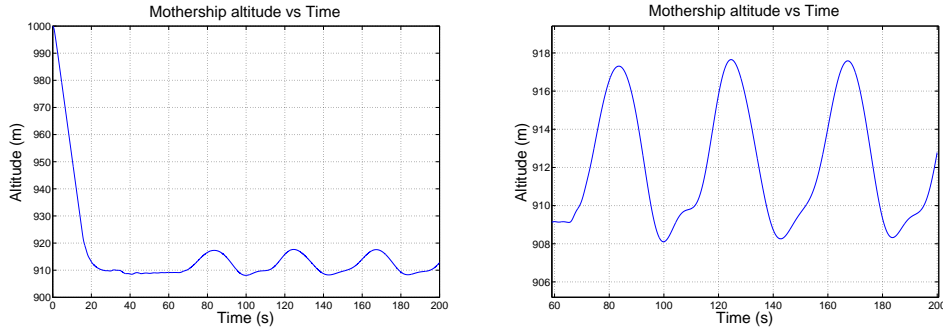


Figure 11: Mothership altitude vs. time under the drogue altitude stabilization using mothership altitude control (left). From the zoomed-in view (right), it can be seen that the mothership has to modulate its altitude ranging within 10 meters to stable the drogue altitude.

unconstrained acceleration \mathbf{a}_d of the drogue is

$$\mathbf{a}_d = \mathbf{g} + \frac{1}{m_d}(\mathbf{D}_d + \mathbf{L}_d),$$

where \mathbf{g} is the gravitational constant at Earth sea level, m_d is the mass of the drogue, and \mathbf{D}_d and \mathbf{L}_d are the aerodynamic drag and lift forces respectively, which equal

$$\begin{aligned} \mathbf{D}_d &= \frac{1}{2}\rho C_D S \|\dot{\mathbf{x}}_d\| \dot{\mathbf{x}}_d \\ \mathbf{L}_d &= \frac{1}{2}\rho C_L S \|\dot{\mathbf{x}}_d\|^2 \mathbf{e}_L, \end{aligned}$$

where ρ is the atmospheric density, S is the incidence area of the drogue, \mathbf{e}_L is the unit vector defining the lift force direction of the drogue in the inertia frame, and C_D and C_L are drag and lift coefficients respectively.

The position constraint of the drogue can be written as

$$\phi(\mathbf{x}_d, \mathbf{x}_m) = \|\mathbf{x}_m - \mathbf{x}_d\|^2 - l^2 = 0,$$

where l is the cable length. The velocity constraint is

$$\psi(\mathbf{x}_d, \mathbf{x}_m) = (\mathbf{x}_m - \mathbf{x}_d)^T (\dot{\mathbf{x}}_m - \dot{\mathbf{x}}_d) = 0.$$

The acceleration constraint can be written as

$$\mathbf{A}\ddot{\mathbf{x}}_d = \mathbf{b},$$

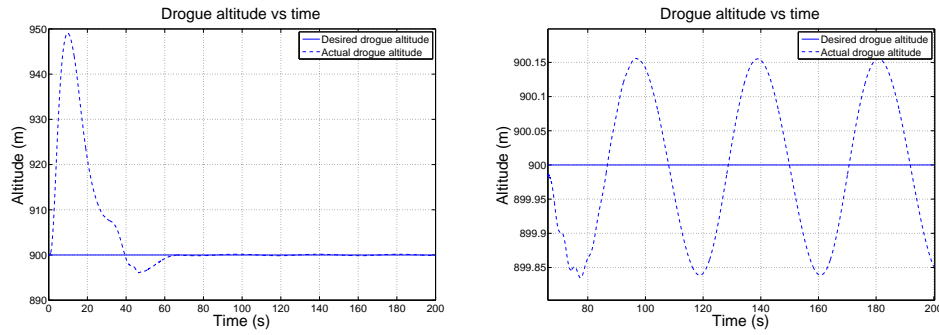


Figure 12: Drogue altitude vs. time in the presence of wind under stable control strategy using cable length regulation (left). From the zoomed-in view (right), it can be seen that in the steady state, the drogue altitude oscillates over the range of 0.32 m approximately.

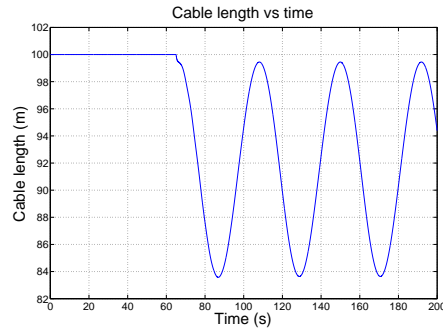


Figure 13: Cable length vs. time in the presence of wind under altitude stabilization using cable length regulation.. The cable length regulation control strategy is switched on at $t = 65\text{ s}$.

where

$$\begin{aligned}\mathbf{A} &= (\mathbf{x}_m - \mathbf{x}_d)^T, \\ \mathbf{b} &= (\mathbf{x}_m - \mathbf{x}_d)^T \ddot{\mathbf{x}}_m + \|\dot{\mathbf{x}}_m - \dot{\mathbf{x}}_d\|^2.\end{aligned}$$

By Gauss's principle, the actual acceleration of the drogue is given by^{1,3,4}

$$\begin{aligned}\ddot{\mathbf{x}}_d &= \mathbf{a}_d + \mathbf{A}^+(\mathbf{b} - \mathbf{A}\mathbf{a}_d) - \gamma_1 \left(\frac{\partial \phi}{\partial \mathbf{x}} \right)^T \phi - \gamma_2 \left(\frac{\partial \psi}{\partial \mathbf{x}} \right)^T \psi \\ &= (\mathbf{I} - \mathbf{A}^+\mathbf{A}) \mathbf{a}_d + \mathbf{A}^+\mathbf{b} - \gamma_1 \left(\frac{\partial \phi}{\partial \mathbf{x}} \right)^T \phi - \gamma_2 \left(\frac{\partial \psi}{\partial \mathbf{x}} \right)^T \psi,\end{aligned}$$

where

$$\begin{aligned}\mathbf{A}^+ &= \mathbf{A}^T (\mathbf{A}\mathbf{A}^T)^{-1} = \frac{\mathbf{x}_m - \mathbf{x}_d}{\|\mathbf{x}_m - \mathbf{x}_d\|^2}, \\ \left(\frac{\partial \phi}{\partial \mathbf{x}} \right)^T &= -2(\mathbf{x}_m - \mathbf{x}_d), \\ \left(\frac{\partial \psi}{\partial \mathbf{x}} \right)^T &= -(\dot{\mathbf{x}}_m - \dot{\mathbf{x}}_d), \\ \mathbf{a}_d &= \mathbf{g} + \frac{\rho S}{2m_d} \|\mathbf{x}_2\| (C_D \mathbf{x}_2 + C_L \|\mathbf{x}_2\| \mathbf{e}_L).\end{aligned}$$

Letting $\mathbf{x} = (\mathbf{x}_1^T, \mathbf{x}_2^T)^T = (\mathbf{x}_d^T, \dot{\mathbf{x}}_d^T)^T$, and $\mathbf{u} = (\mathbf{x}_m^T, \dot{\mathbf{x}}_m^T, \ddot{\mathbf{x}}_m^T, \mathbf{a}_d^T)^T$, we obtain the continuous dynamic

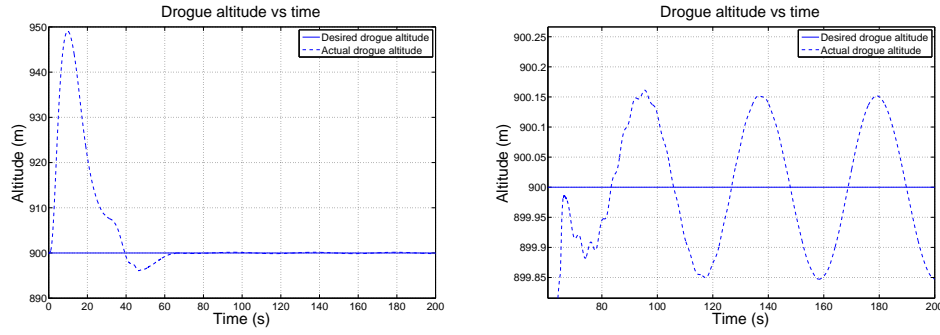


Figure 14: Drogue altitude vs. time in the presence of wind under altitude stabilization using both mothership altitude control and cable length regulation (left). From the zoomed-in view (right), it can be seen that in the steady state, the drogue altitude oscillates over the range of approximately 0.3 m .

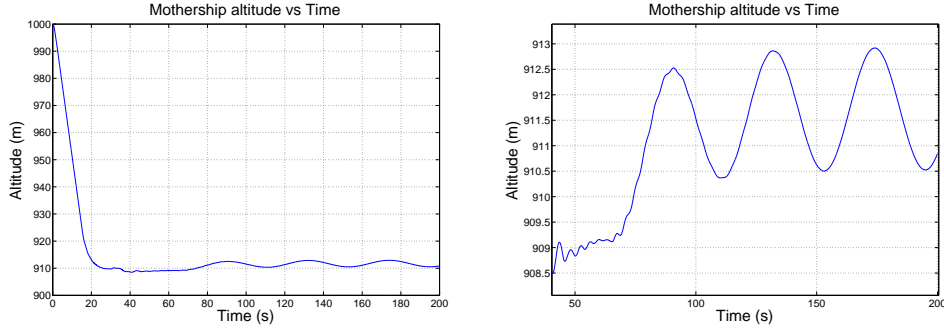


Figure 15: Mothership altitude vs time in the presence of wind under altitude stabilization using both mothership altitude control and cable length regulation (left). From the zoomed-in view (right), it can be seen that in the steady state, the modulation of the mothership altitude ranges within 3 meters.

equations for drogue motion as

$$\begin{aligned} \dot{\mathbf{x}} &= \begin{pmatrix} \mathbf{x}_2 \\ (\mathbf{I} - \mathbf{A}^+ \mathbf{A}) \mathbf{a}_d + \mathbf{A}^+ \mathbf{b} - \gamma_1 \left(\frac{\partial \phi}{\partial \mathbf{x}} \right)^T \phi - \gamma_2 \left(\frac{\partial \psi}{\partial \mathbf{x}} \right)^T \psi \end{pmatrix} \\ \mathbf{y} &= \mathbf{x}_1. \end{aligned} \quad (3)$$

Discretizing Equation (3) we have

$$\begin{aligned} \mathbf{x}_k &= \mathbf{f}(\mathbf{x}_{k-1}, \mathbf{u}_k) \\ \mathbf{y}_k &= \mathbf{h}(\mathbf{x}_k), \end{aligned}$$

where

$$\begin{aligned} \mathbf{f}(\cdot) &= \mathbf{x}_{k-1} + \Delta T \cdot \begin{pmatrix} \mathbf{x}_2 \\ \ddot{\mathbf{x}}_d \end{pmatrix}_{k-1} \\ \mathbf{h}(\cdot) &= \mathbf{x}_k, \end{aligned} \quad (4)$$

and where ΔT is the sample time.

The Jacobians of Equation (4) can be written as

$$\begin{aligned} \mathbf{F}_k &= \frac{\partial \mathbf{f}}{\partial \mathbf{x}} = \begin{bmatrix} \frac{\partial f_1}{\partial \mathbf{x}_1} & \frac{\partial f_1}{\partial \mathbf{x}_2} \\ \frac{\partial f_2}{\partial \mathbf{x}_1} & \frac{\partial f_2}{\partial \mathbf{x}_2} \end{bmatrix}, \\ \mathbf{H}_k &= \frac{\partial \mathbf{h}}{\partial \mathbf{x}}, \end{aligned}$$

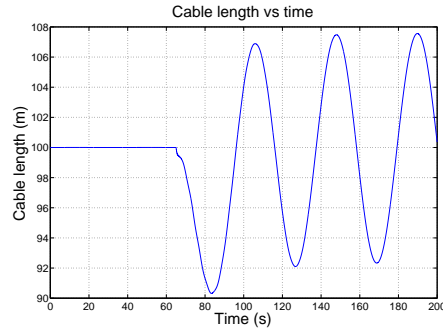


Figure 16: Cable length vs. time in the presence of wind under altitude stabilization using both mothership altitude control and cable length regulation.. The cable length regulation control strategy is switched on at $t = 65$ s

where

$$\begin{aligned}\frac{\partial f_1}{\partial \mathbf{x}_1} &= \frac{\partial}{\partial \mathbf{x}_1} (\mathbf{x}_1 + \Delta T \cdot \mathbf{x}_2) = \mathbf{I}_3, \\ \frac{\partial f_1}{\partial \mathbf{x}_2} &= \frac{\partial}{\partial \mathbf{x}_2} (\mathbf{x}_1 + \Delta T \cdot \mathbf{x}_2) \\ &= \Delta T \cdot \mathbf{I}_3, \\ \frac{\partial f_2}{\partial \mathbf{x}_1} &= \frac{\partial}{\partial \mathbf{x}_1} (\mathbf{x}_2 + \Delta T \cdot \ddot{\mathbf{x}}_d) \\ &= \Delta T \cdot \frac{\partial \ddot{\mathbf{x}}_d}{\partial \mathbf{x}_1}, \\ \frac{\partial f_2}{\partial \mathbf{x}_2} &= \frac{\partial}{\partial \mathbf{x}_2} (\mathbf{x}_2 + \Delta T \cdot \ddot{\mathbf{x}}_d) \\ &= \mathbf{I}_3 + \Delta T \cdot \frac{\partial \ddot{\mathbf{x}}_d}{\partial \mathbf{x}_2}.\end{aligned}$$

Letting

$$\ddot{\mathbf{x}}_d = \Gamma_1 + \Gamma_2 + \Gamma_3 + \Gamma_4,$$

where

$$\begin{aligned}\Gamma_1 &= \mathbf{a}_d + \frac{(\mathbf{x}_m - \mathbf{x}_1)(\mathbf{x}_m - \mathbf{x}_1)^T}{\|\mathbf{x}_m - \mathbf{x}_1\|^2} (\ddot{\mathbf{x}}_m - \mathbf{a}_d), \\ \Gamma_2 &= \frac{(\mathbf{x}_m - \mathbf{x}_1) \|\dot{\mathbf{x}}_m - \dot{\mathbf{x}}_2\|^2}{\|\mathbf{x}_m - \mathbf{x}_1\|^2}, \\ \Gamma_3 &= 2\gamma_1(\mathbf{x}_m - \mathbf{x}_1) \left(\|\mathbf{x}_m - \mathbf{x}_1\|^2 - l^2 \right), \\ \Gamma_4 &= \gamma_2(\dot{\mathbf{x}}_m - \dot{\mathbf{x}}_2)(\mathbf{x}_m - \mathbf{x}_1)^T (\dot{\mathbf{x}}_m - \dot{\mathbf{x}}_2).\end{aligned}$$

Reference 5 gives us the product rule for the derivative of a matrix with respect to a matrix, which is, for the matrices $\mathbf{X}_{m \times n}$, $\mathbf{Y}_{n \times v}$, $\mathbf{Z}_{p \times q}$,

$$\frac{\partial(\mathbf{X}\mathbf{Y})}{\partial \mathbf{Z}} = \frac{\partial \mathbf{X}}{\partial \mathbf{Z}} (\mathbf{I}_p \otimes \mathbf{Y}) + (\mathbf{I}_q \otimes \mathbf{X}) \frac{\partial \mathbf{Y}}{\partial \mathbf{Z}}, \quad (5)$$

where \otimes denotes Kronecker product. To calculate $\frac{\partial \ddot{\mathbf{x}}_d}{\partial \mathbf{x}_1}$ and $\frac{\partial \ddot{\mathbf{x}}_d}{\partial \mathbf{x}_2}$, we need to investigate the partial derivatives of the each part of $\ddot{\mathbf{x}}_d$ with respect to \mathbf{x}_1

$$\frac{\partial \ddot{\mathbf{x}}_d}{\partial \mathbf{x}_1} = \frac{\partial \Gamma_1}{\partial \mathbf{x}_1} + \frac{\partial \Gamma_2}{\partial \mathbf{x}_1} + \frac{\partial \Gamma_3}{\partial \mathbf{x}_1} + \frac{\partial \Gamma_4}{\partial \mathbf{x}_1},$$

and since $\frac{\partial \mathbf{a}_d}{\partial \mathbf{x}_1} = \frac{\partial \ddot{\mathbf{x}}_m}{\partial \mathbf{x}_1} = \mathbf{0}_{3 \times 3}$, so

$$\begin{aligned}\frac{\partial \Gamma_1}{\partial \mathbf{x}_1} &= \frac{\partial}{\partial \mathbf{x}_1} \left(\frac{(\mathbf{x}_m - \mathbf{x}_1)(\mathbf{x}_m - \mathbf{x}_1)^T}{\|\mathbf{x}_m - \mathbf{x}_1\|^2} (\ddot{\mathbf{x}}_m - \mathbf{a}_d) \right) \\ &= -\frac{1}{\|\mathbf{x}_m - \mathbf{x}_1\|^2} \left((\mathbf{x}_m - \mathbf{x}_1)^T (\ddot{\mathbf{x}}_m - \mathbf{a}_d) \mathbf{I}_3 + (\mathbf{x}_m - \mathbf{x}_1) (\ddot{\mathbf{x}}_m - \mathbf{a}_d)^T \right) \\ &\quad + \frac{2}{\|\mathbf{x}_m - \mathbf{x}_1\|^4} (\mathbf{x}_m - \mathbf{x}_1)(\mathbf{x}_m - \mathbf{x}_1)^T \cdot (\ddot{\mathbf{x}}_m - \mathbf{a}_d) (\mathbf{x}_m - \mathbf{x}_1)^T.\end{aligned}$$

Similarly, we can obtain

$$\frac{\partial \Gamma_2}{\partial \mathbf{x}_1} = \frac{1}{\|\mathbf{x}_m - \mathbf{x}_1\|^2} \left(-\mathbf{I}_3 \cdot \|\dot{\mathbf{x}}_m - \mathbf{x}_2\|^2 \right) + \frac{2}{\|\mathbf{x}_m - \mathbf{x}_1\|^4} (\mathbf{x}_m - \mathbf{x}_1) \|\dot{\mathbf{x}}_m - \mathbf{x}_2\|^2 \cdot (\mathbf{x}_m - \mathbf{x}_1)^T,$$

$$\frac{\partial \Gamma_3}{\partial \mathbf{x}_1} = -2\gamma_1 \left(\mathbf{I}_3 \cdot \left(\|\mathbf{x}_m - \mathbf{x}_1\|^2 - l^2 \right) + 2(\mathbf{x}_m - \mathbf{x}_1) \cdot (\mathbf{x}_m - \mathbf{x}_1)^T \right),$$

$$\frac{\partial \Gamma_4}{\partial \mathbf{x}_1} = -\gamma_2 (\dot{\mathbf{x}}_m - \mathbf{x}_2) (\dot{\mathbf{x}}_m - \mathbf{x}_2)^T,$$

thus, we can obtain $\frac{\partial \ddot{\mathbf{x}}_d}{\partial \mathbf{x}_1}$. Similarly, we can calculate

$$\frac{\partial \ddot{\mathbf{x}}_d}{\partial \mathbf{x}_2} = \frac{\partial}{\partial \mathbf{x}_2} (\mathbf{a}_d + \Gamma_2 + \Gamma_4),$$

where

$$\frac{\partial \mathbf{a}_d}{\partial \mathbf{x}_2} = \frac{\rho S C_D}{2m_d} \cdot \left(\|\mathbf{x}_2\| \mathbf{I}_3 + \frac{\mathbf{x}_2 \mathbf{x}_2^T}{\|\mathbf{x}_2\|} \right) + \frac{\rho S C_L}{m_d} \mathbf{e}_L \mathbf{x}_2^T,$$

$$\frac{\partial \Gamma_2}{\partial \mathbf{x}_2} = -\frac{2(\mathbf{x}_m - \mathbf{x}_1) (\dot{\mathbf{x}}_m - \mathbf{x}_2)^T}{\|\mathbf{x}_m - \mathbf{x}_1\|^2},$$

$$\frac{\partial \Gamma_4}{\partial \mathbf{x}_2} = -\gamma_2 \left((\mathbf{x}_m - \mathbf{x}_1)^T (\dot{\mathbf{x}}_m - \mathbf{x}_2) \cdot \mathbf{I}_3 + (\dot{\mathbf{x}}_m - \mathbf{x}_2) (\mathbf{x}_m - \mathbf{x}_1)^T \right).$$

We also can calculate

$$\begin{aligned}\mathbf{H}_k &= \frac{\partial \mathbf{h}}{\partial \mathbf{x}} \\ &= \mathbf{I}_6.\end{aligned}$$

B. Simulation results

We develop several simulations with different time delays to verify the EKF estimator derived in the previous section. Assuming that after certain steps of the sample time, the estimator obtains the measured data from the drogue sensor. Figure 17 depicts the estimated drogue altitudes compared to the real ones. It can be seen that with the increasing of the time delay, the estimated values of the drogue altitude becomes increasingly noisy. The result illustrates that the EKF estimator can be used in the situation of GPS data delay for the situation of small time delay.

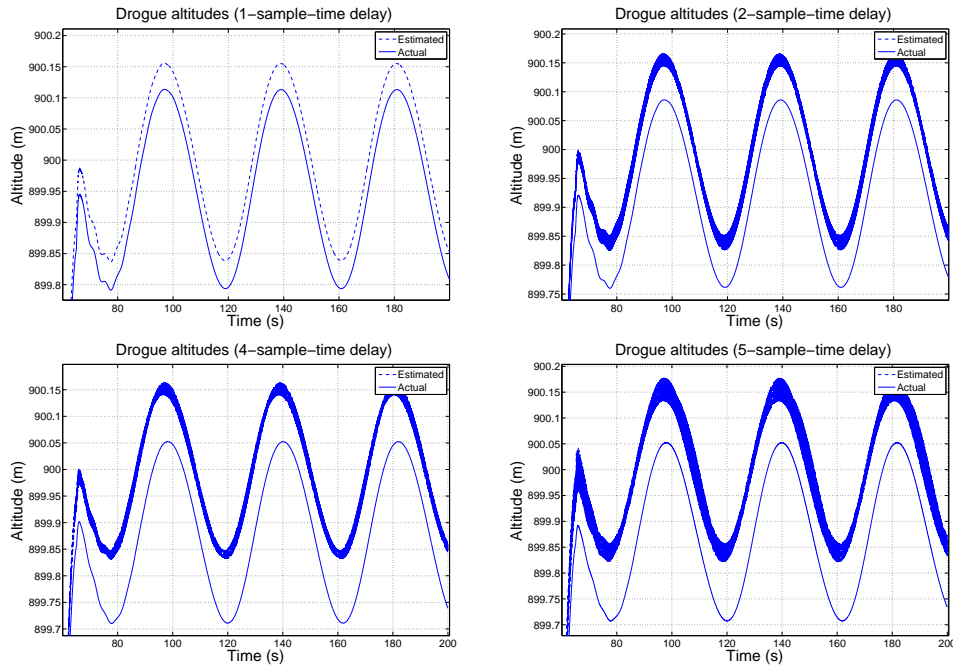


Figure 17: The estimated and real data of drogue altitude vs time with different time delays.

V. Conclusion

In this paper we presented the preliminary flight test results which verify the feasibility of the concept of the aerial recovery. Based on results of the simulation in which we tried to match the flight test results, the mathematical model is testified to be suitable for further study of the system. Applying the established simulation environment, a series of trade studies are conducted and the results show that the drogue mass, drogue drag coefficient and cable length are key parameters which affect the steady state of the system. Two control strategies to stabilize the drogue altitude in the presence of steady wind are developed and the simulation results show that the approach of cable length regulation is better than that of mothership altitude control. However the feasibility of the cable length regulation in the flight test needs further exploration. The Extended Kalman Filter for drogue states estimation in the case of data delay is developed and the simulation results show the feasibility of the estimator in small time delay.

VI. Acknowledgment

This research was supported by the Air Force Office of Scientific Research under STTR contract No. FA 9550-09-C-0102 to Procerus Technologies and Brigham Young University. The flight test results are obtained under the help of Dr. Mark B. Colton, Daniel C. Carlson and Jesse Williams.

References

- ¹Sun, L., Beard, R. W., Colton, M. B., and McLain, T. W., "Dynamics and Control of Cable-Drogue System in Aerial Recovery of Micro Air Vehicles Based on Gauss's Principle," 2009 American Control Conference, St. Louis, MO, USA, June 2009, pp. 4729–4734.
- ²Murray, R., "Trajectory Generation For a Towed Cable System Using Differential Flatness," *13th Triennial World Congress of the International Federation of Automatic Control*, 1996, pp. 395–400.
- ³Udwadia, F. E. and Kalaba, R. E., *Analytical Dynamics: A New Approach*, Cambridge University Press, 1996.
- ⁴McLain, T. W. and Beard, R. W., "Trajectory Planning for Coordinated Rendezvous of Unmanned Air Vehicles," Vol. 4369, 2000, pp. 1–8.
- ⁵Graham, A., *Kronecker Products and Matrix Calculus: with Applications*, Chichester: Horwood, 1981.